From BCS-like superconductivity to condensation of local pairs: A numerical study of the attractive Hubbard model

J. M. Singer
Physik-Institut, Universität Zürich, Winterthurerstrasse 190, CH-8057 Zürich, Switzerland

M. H. Pedersen and T. Schneider
IBM Research Division, Zurich Research Laboratory, CH-8803 Rüschlikon, Switzerland

H. Beck
Institut de Physique, Université de Neuchâtel, Rue A.L. Breguet 1, CH-2000 Neuchâtel, Switzerland

H.-G. Matuttis
Institut für Computeranwendungen I, Universität Stuttgart, Pfaffenwaldring 27, D-70569 Stuttgart, Germany
(Received 1 February 1996)

We investigate the two-dimensional attractive Hubbard model with quantum Monte Carlo techniques to reveal the crossover from a BCS-type superconductivity in the weak-coupling regime to a superconductivity properly described by a Bose-Einstein condensation (BEC) of local, preformed pairs. The crossover from BCS to BEC is particularly well exposed in the temperature dependence of both the spin susceptibility and the double occupancy, as well as by the appearance of a pseudogap in the density of states far above T_c. These features are also mirrored in the shape of the specific-heat peak around T_c, the separation of the temperature regimes where pair formation and their condensation occur, and in the transfer of spectral weight from the single-particle excitation branch to a pair band in the normal state. [S0163-1829(96)05226-5]

I. INTRODUCTION

The main purpose of this work is to explore the crossover in the attractive Hubbard model from weak- to strong-coupling superconductivity. In the weak-coupling regime a BCS description (see, e.g., Ref. 1) is adequate and the occurrence of superconductivity below the critical temperature T_c is tied to a pairing instability of the Fermi liquid at T_c. The formation and condensation of pairs only occur below T_c. In the strong-coupling limit, however, the scenario of Bose-Einstein condensation (BEC) appears to be more adequate because the pairs that condensate at T_c already occur at a higher temperature. Accordingly, we expect that the normal-state properties of these limiting coupling regimes will differ markedly. In phase-transition terminology, the weak-coupling regime corresponds to the limit where a mean-field description becomes valid, because the neglect of superconducting fluctuations in the normal state is justified. In the strong-coupling or BEC regime, superconducting fluctuations dominate in a temperature window around T_c and, most importantly, also occur above T_c. The crossover from weak- to strong-coupling superconductivity corresponds in this respect to a crossover from mean-field to fluctuation-dominated or critical-point behavior. In this context it is interesting to note that, in an early attempt prior to BCS, Blatt and Schafroth[2] explored BEC in the ideal and charged boson gas to understand the occurrence of superconductivity in conventional metals. An important similarity throughout the coupling range is that we can, for instance, apply Yang's concept[3] of off-diagonal long-range order (ODLRO) in the reduced density matrix to classify the macroscopic quantum state.

Renewed interest in this crossover arose with the discovery and study of high-T_c materials. Unlike conventional BCS superconductors, these compounds are characterized by extremely small pairs having a spatial extension of the order of one lattice spacing. For this reason the high-T_c materials have been attributed to the intermediate-coupling regime.[4] This crossover has been studied by various authors[4–7] and, more recently, by Randeria *et al.*[8–10]

Our intention here is to extend these studies. We concentrate on the investigation of the attractive Hubbard model with two types of quantum Monte Carlo (QMC) methods, the grand-canonical approach after Hirsch[11] for the $T>0$ regime and the projector method for the ground state. The implementation of recent improvements of the numerical tools (see Ref. 12) allows us to extend this QMC study far beyond the previously published data. We can easily reach sufficiently large cluster sizes (Sec. III presents data for lattices up to 144 sites), achieve high coupling strengths of up to $U/t=-12$ and even higher, and cover the entire temperature range down to the ground state. Our extension of previous QMC results includes the dependence of a rather long list of properties on temperature, band filling, and coupling strength. These properties include kinetic energy, double occupancy, specific heat, spin susceptibility, superconducting order parameters, chemical potential, and the one-particle spectral functions. In Sec. II we introduce the model. A brief outline of the QMC method is given in Sec. III. To provide guidelines for the interpretation of the QMC results, we sketch in Sec. IV the BCS and moment approaches. In Sec. V we present and discuss our QMC results. The crossover from BCS to BEC is particularly well exposed in the temperature dependence of both the spin susceptibility and the

double occupancy, as well as the appearance of a pseudogap in the density of states far above T_c. These features are also mirrored in the shape of the specific-heat peak around T_c, the separation of the temperature regimes where pair formation and their condensation occurs, and in the transfer of spectral weight from the single-particle excitation branch to a pair band in the normal state.

II. MODEL

As a starting point for our investigation we use the well-known two-dimensional attractive Hubbard model (''negative-U model'') on a square lattice:

$$\mathcal{H} = -t \sum_{\langle ij \rangle \sigma} (c_{i\sigma}^{\dagger} c_{j\sigma} + \text{H.c.}) + U \sum_{i} n_{i\uparrow} n_{i\downarrow} - \mu \sum_{i\sigma} n_{i\sigma}, \tag{1}$$

where $c_{i\sigma}^{\dagger}$ ($c_{i\sigma}$) denote fermionic creation (annihilation) operators at site i with spin σ, and t is the kinetic term between two neighboring sites, which serves as an energy unit throughout the paper. The limit $\langle ij \rangle$ restricts the sum to next neighbors, U denotes the interaction (''coupling''), which is repulsive for positive and attractive for negative values of strength U, and μ is the chemical potential.

In the free case ($U/t = 0$) we have the well-known dispersion relation for the two-dimensional system

$$\epsilon(k) = -2t[\cos(k_x) + \cos(k_y)]. \tag{2}$$

This system is the simplest lattice model for correlated electrons which can become superconducting, and it is believed to undergo in two dimensions (2D) a Kosterlitz-Thouless (KT) transition into a superconducting s-wave state away from half-filling. At half-filling one finds a coexistence of superconducting and long-range charge-density wave correlations, which drive the effective KT transition temperature in 2D to zero, $T_{\mathrm{KT}}(\rho = 0.5) = 0$.[13,14] The phase diagram is symmetric around half-filling, $\rho = 0.5$ (density per site and per spin, filling $\langle n \rangle = 1.0$ electrons per site), i.e., $T_{\mathrm{KT}}(\rho) = T_{\mathrm{KT}}(1-\rho)$, because of particle-hole symmetry, and reaches its maximum around $\rho = 0.4\ T_{\mathrm{KT}}$.

Because of its simplicity this model allows us to investigate a remarkable crossover from low to strong interaction. Varying the U parameter provides us with a tuning instrument for the pair size and therefore for a transition from highly extended pairs to more or less local pairs. Nevertheless we do not propose this model as a realistic high-T_c model, but use it to gain a better understanding of the basic mechanisms at the superconducting transition.

III. QUANTUM MONTE CARLO METHODS

We present numerical studies of the described model using predominantly two types of QMC methods, the grand canonical QMC formalism after Hirsch,[11] and the projector QMC method based on earlier work by Sugiyama and Koonin, Sorella *et al.*, and de Raedt.[15–17] We emphasize that the QMC approach has the potential to treat these types of strongly correlated systems, allowing us to go far beyond certain approximative methods; it provides an approximation-free, numerically exact ansatz, unlike most standard analytical techniques, and yields information about systems much larger than those accessible by exact diagonalization algorithms. In addition, applying these methods to the attractive Hubbard model frees us from the central drawback of fermion QMC calculations, the so-called ''sign problem.'' This allows us to perform reliable and stable calculations over a vast parameter range. For both methods we use the Suzuki-Trotter and the Hubbard-Stratonovich transformation to ''break up'' the quantum-mechanical many-particle system.

A central technique on which we rely is the temperature-dependent formulation of a QMC algorithm in the grand-canonical ensemble, which is largely based on the work of Hirsch.[11] Most of the presented data were produced with this method. It starts with the grand-canonical formulation of the partition function Z, the expectation value for a certain quantum-mechanical observable O then represents an average over the grand canonical ensemble as

$$\langle O \rangle = \frac{1}{Z} \mathrm{Tr}(O \exp(-\beta H)) \tag{3}$$

with the partition function

$$Z = \mathrm{Tr}(\exp(-\beta H)). \tag{4}$$

But this ansatz has a weak point:

For large β, i.e., at low temperatures, the grand canonical algorithm of Hirsch[18] becomes increasingly useless because not only the numerical effort to go to higher β values (i.e., to lower temperatures) itself increases the computer time, but also because numerical instabilities start to dominate in the low-temperature regime and the necessary amount of CPU time to compensate them by introducing more and more sophisticated stabilization techniques[12,19,20] grows dramatically.

Although we are able to push our algorithm to far lower temperatures than usually known in the literature, we prefer to switch to a different type of QMC method to investigate the ground-state properties of the system, now in the canonical ensemble with fixed particle numbers. For this purpose we apply the projector method,[15–17,21] which enables us to filter out the ground state of a wave function by applying a projector/filter $\exp(-\Theta\mathcal{H})$ (in imaginary time) to an appropriate test or trial wave function $|\Psi_T\rangle$, where it is supposed that the trial function has a nonvanishing overlap with the ground state. By expanding in energy eigenvalues one can show that all states $|\Psi_1\rangle, |\Psi_2\rangle, \ldots$ that belong to higher energies than the ground state $|\Psi_0\rangle$ are exponentially suppressed:

$$\begin{aligned} \exp(-\Theta\mathcal{H})|\Psi_T\rangle &= \exp(-\Theta\mathcal{H}) \sum_n |\Psi_n\rangle\langle\Psi_n|\Psi_T\rangle \\ &= \exp(-\Theta E_0) \Big\{ \langle\Psi_0|\Psi_T\rangle|\Psi_0\rangle \\ &\quad + \sum_{n>0} \exp[-\Theta(E_n - E_0)] \\ &\quad \times \langle\Psi_n|\Psi_T\rangle|\Psi_n\rangle \Big\} \\ &\overset{\Theta\to\infty}{\to} C \cdot |\Psi_0\rangle. \end{aligned}$$

The exponential of the Hamiltonian $\exp(-\Theta\mathcal{H})$ can again be treated using the two above-mentioned decompositions, and again we are faced with certain numerical instabilities, which we now try to suppress by applying a modified Gram-Schmidt scheme as introduced by Sorella.[16]

For both methods we use as updating mechanism a special single-spin algorithm, which allows a very efficient and elegant formulation of the algorithm.[12,22] Both methods provide us primarily with equal-time normal Green's functions, which we denote $\langle c_i c_j^\dagger \rangle$, and which we can use to compute a large number of observables such as the energies, occupation numbers, susceptibilities, and space-resolved pair-correlation functions to investigate the normal-state and superconducting properties of our system.

According to Yang[3,23–25] the relevant order parameter for the examination of the superconducting properties is the reduced two-particle density matrix or rather the pair-field correlation function; because the attractive Hubbard model is believed to undergo a transition into a s-wave state we concentrate merely on the following observable:

$$\chi_{xs}(l)=\langle \Delta_m^\dagger(0)\Delta_m(l)+\Delta_m(0)\Delta_m^\dagger(l)\rangle, \tag{5}$$

where

$$\Delta_m^\dagger(l)=\frac{1}{N}\sum_i\ c_{i+l+m/2}^\dagger c_{i+l-m/2}^\dagger. \tag{6}$$

We call $m=0$ the on-site pair operator, where both constituents of the pair are created at the same site and annihilated at distance l; analogously we can investigate larger pair extensions $m=1,\sqrt{2},\ldots,$ which we call ''extended-s pairs.'' To exclude trivial one-particle contributions we focus on the so-called ''vertex'' correlation function[26] by substracting the corresponding one-particle contributions. In other words we calculate the difference of the (in fermionic operators) quartic contributions and the product of the quadratic contributions. A macroscopic quantum state, i.e., superconductivity, is indicated by off-diagonal long-range order (ODLRO),[3,23–25] which is present if the vertex correlation function approaches a finite constant value (''plateau value'') for large spatial pair distances; we use this long-range plateau value (in the following sections denoted ''plateau'' or $\chi_{\rm os}^{\rm plateau}$) as a substitute for a superconducting order parameter

$$\chi(l)=\chi^{\rm plateau}+\exp(-l/\xi). \tag{7}$$

In addition we are able to retrieve in both frameworks time-dependent Green's functions (in imaginary time), which may be written

$$G_\sigma(i-j,\tau)=-\langle T_\tau c_{i\sigma}(\tau)c_{j\sigma}^\dagger(0)\rangle. \tag{8}$$

As we are merely interested in dynamical properties at finite temperatures, we restrict ourselves to the evaluation of this quantity in the grand canonical algorithm; a scheme for the application in the $T=0$ formalism was introduced by von der Linden[26] and applied in Refs. 12 and 27.

The time-dependent Green's functions $G(k,\tau)$ in k space are intimately connected to the spectral function $A(k,\omega)$ via

$$G(k,\tau)=\begin{cases} -\displaystyle\int_{-\infty}^{\infty} d\omega\,\frac{\exp(-\omega\tau)}{\exp(-\beta\omega)+1}A(k,\omega) & \text{if } \tau>0; \\ +\displaystyle\int_{-\infty}^{\infty} d\omega\,\frac{\exp(-\omega\tau)}{\exp(+\beta\omega)+1}A(k,\omega) & \text{if } \tau<0, \end{cases} \tag{9}$$

from which we can easily obtain the density of states as a summation over all k states:

$$N(\omega)=\frac{1}{N}\sum_k\ A(k,\omega). \tag{10}$$

These simple equations pose a serious problem: It is rather difficult to extract the spectral properties from the computed QMC data because an analytic continuation, or rather an inverse Laplace transformation from imaginary to real time, is required. This inversion of QMC data (and usually of all statistically computed data) is extremely numerically ill-posed due to two obvious reasons: Data are available only for a limited set of imaginary times and the data are usually more or less noisy. As a consequence, the solution might not be unique in general.

The method of choice is the maximum entropy ansatz, as proposed by Gubernatis, Jarrell and co-workers[27–30] for a similar type of data; the method we used to obtain the presented information is a slight variation of this ansatz after von der Linden's work.[27,31]

IV. ALTERNATIVE METHODS

We use the recent generalization of Nolting's moment approach[32–34] to study the single-particle properties of the negative-U model in the normal state as well as in the superconducting regime. Adapting a two-δ-peak ansatz $(j=2)$ for the spectral density $A(k,\omega)$ in the normal state and a four-δ-peak ansatz $(j=4)$ in the superconducting regime

$$A(k,\omega)=\sum_{i=1}^{j}\ \alpha_i(k)\,\delta(\omega-\Omega_i(k)), \tag{11}$$

one is able to fix the resulting excitation branches and their weights in terms of the exact first four normal moments

$$A_n(k)=\int_{-\infty}^{\infty} d\omega\omega^n A(k,\omega) \tag{12}$$

and the first two anomalous frequency moments $B_n(k)$. This leads to a set of self-consistently solvable equations for the parameters including the chemical potential and the gap for fixed band filling and temperature. A crucial limitation of this approach arises from the neglect of damping in the two excitation branches, i.e., lifetime effects and multiparticle excitations (continuum states) are not included. This ansatz correctly reproduces the atomic limit, the free case and the strong-coupling limit in first order of t. In the intermediate-coupling regime it provides reasonable estimates as long as the chemical potential is within a band. Further details can be found in Refs. 33 and 34.

In addition we include a result from a self-consistent T-matrix approach;[35] unfortunately this method allows only

valuable results in the low-correlation limit, i.e., low filling and weak coupling as discussed in the Sec. V because it involves only two-particle interaction terms and neglects such features as the particle-hole interaction channel. We nevertheless find that it provides a very interesting approach to compare our results and to clarify limitations of the QMC ansatz, especially because this method gives access to remarkably larger lattice sizes, which might be an important feature for the investigation of quantities such as spectral weights or the density of states. As a consequence it provides quite good access to the limit of very low coupling strength $-4t<U<0$, which is difficult to treat by QMC due to more or less severe finite-size effects.

We also compared our results with the BCS approximation yielding the gap equation

$$\frac{1}{U}=\sum_k \frac{1}{2E_k}\tanh\left(\frac{\beta E_k}{2}\right) \tag{13}$$

with the extended dispersion

$$E_k=\sqrt{(\epsilon_k-\overline{\mu})^2+\Delta^2}, \tag{14}$$

where ϵ_k is the dispersion in the noninteracting case, Δ the gap, $\overline{\mu}=\mu-\rho U$ the chemical potential including a Hartree shift, and U the strength of the attractive interaction. Because Δ vanishes at and above T_c, the gap equation also fixes the transition temperature.

Moreover, the chemical potential follows from

$$\rho=\sum_k [\exp(\beta(E_k-\overline{\mu}))+1]^{-1}, \tag{15}$$

and the spin susceptibility is given by

$$\chi_{s,0}=2\beta\sum_k \frac{\exp(\beta E_k)}{[1+\exp(\beta E_k)]^2}. \tag{16}$$

For the spin susceptibility, a simple random-phase approximation (RPA) yields the expression

$$\chi_{s,\mathrm{RPA}}=\frac{\chi_{s,0}}{1-U\chi_{s,0}}, \tag{17}$$

which reduces for $U=0$ to the free-system case $\chi_{s,0}$.

V. RESULTS

Previous investigations revealed the following properties of the 2D attractive Hubbard model: It shows superconducting correlations over the entire filling range; away from half-filling it is believed to undergo a KT transition into a superconducting state, with an estimated maximum T_c around $\rho\approx 0.4$. At and close to half-filling this system also exhibits long-range charge-density correlations, and is widely regarded to be a charge-density insulator, with the consequence that T_c would be driven to zero.[4,13,14,36]

A. Weak-coupling regime

We shall first consider the ''low-correlation'' limit, i.e., $\rho=0.1$ and the interaction strength $U/t=-4.0$, to allow a comparison with the moment, the T-matrix and the BCS approach. This choice of the parameters is motivated by the following considerations.

A sufficiently large attractive interaction leads to a small pair size and coherence length, which reduce the finite-size effects in our simulation of small discrete clusters. For smaller U we found strong size effects, which we can only overcome by a very CPU-time-consuming scaling analysis. In this filling regime, $U/t=-4.0$ turned out to be large enough to produce pairs of the order of only a few lattice spacings, being suitable for lattice sizes accessible to our algorithm, such as 12×12.

Our other restriction was to find a regime that allows a comparison with other methods, such as the moment and

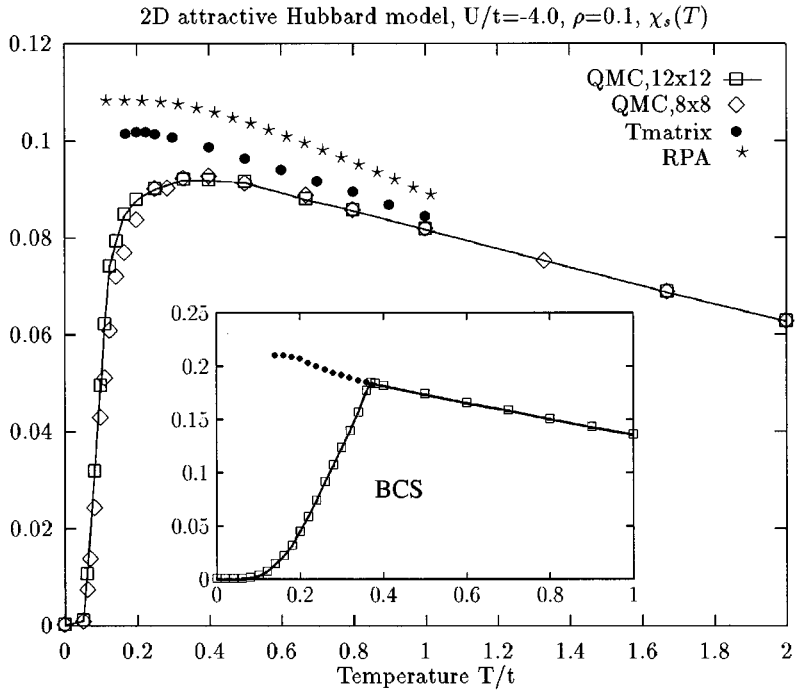

FIG. 1. Uniform magnetic susceptibility χ_s as a function of temperature, $U/t=-4.0$, filling per site and spin $\rho=0.1$ (i.e., 80% doping away from half-filling). Shown is QMC data for two lattice sizes (8×8 and 12×12, open symbols) as well as data from a normal-state T-matrix ansatz above T_c (32×32 lattice, filled circles) and a simple RPA approach (stars). The inset adds data from a BCS treatment of a lattice fermion system, as described in Sec. IV, whereas the filled circles in the inset indicate the continuation of the χ data in the free case, without any BCS gap, for comparison. Note the absence of a fluctuation region in the BCS description.

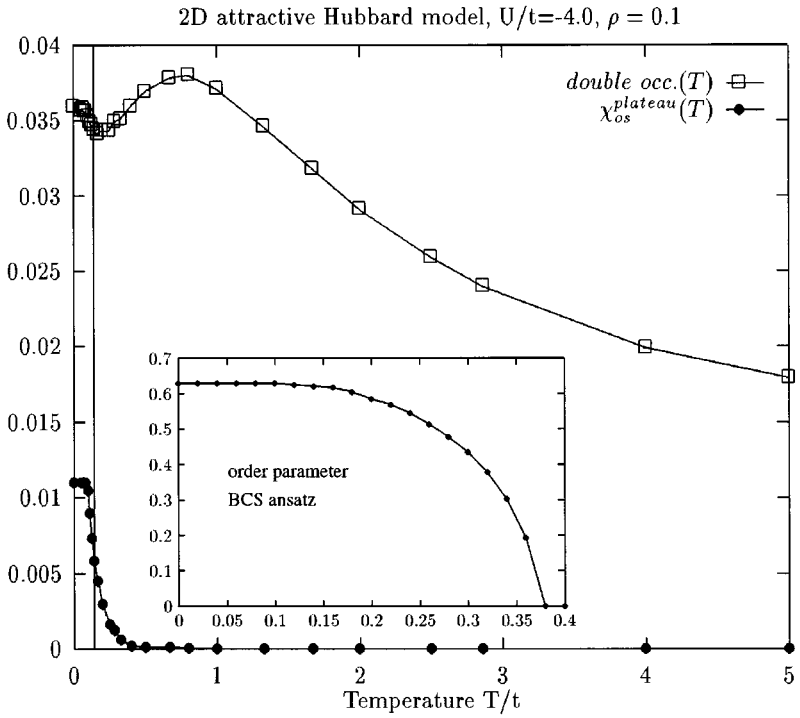

FIG. 2. Double occupancy $\langle n_{i\uparrow} n_{i\downarrow} \rangle$ (open squares) and order parameter (plateau value of the singlet s-pair correlation function, filled circles as a function of temperature. QMC data $U/t = -4.0$, $\rho = 0.1$, system size 12×12. The vertical line marks the transition; one finds a clear signal at the transition temperature in the double occupancy corresponding to the increase of the order parameter. The inset shows the temperature dependence of the superconducting gap within the BCS ansatz for the same parameter set with a much higher transition temperature.

T-matrix approaches. The range of validity of these techniques is the low-correlation limit.

The first quantity we investigated is the uniform static spin susceptibility $\chi_s(T)$, Fig. 1. This figure contains QMC data from two different cluster sizes, as well as self-consistent T-matrix results from Micnas *et al.*,[35] a simple RPA curve, and data from a BCS ansatz in the inset. The T matrix has been evaluated only in the normal state. For large temperatures, the QMC results appear to resemble the T matrix and RPA results quite well, whereas for lower temperatures we find rather pronounced deviations. Below $T/t < 0.5$ even T matrix and QMC deviate strongly because the T-matrix results above T_c show no strong qualitative deviation from RPA and appear to be fairly constant. In contrast, the QMC curves start to bend down at $T/t \approx 0.5$, an astonishingly high temperature, diverging from the usual Pauli behavior, and goes to zero in the superconducting region after a large transition area. The QMC estimate for the transition temperature of this system seems to be at or even below $T/t = 0.1$ (for comparison, see Fig. 2). We would like to associate this behavior with a pair-breaking effect around the critical temperature, which might arise either from a fluctuating superconductivity above T_c or a formation of bound pairs above T_c. We will comment on the possible origin of this effect below. Obviously neither of these effects is accessible by a simple RPA treatment; the normal-state T matrix does not seem to be sufficiently sensitive to these effects, either.

Figure 2 shows QMC results (we henceforth use the convention that all results are QMC data unless explicitly stated otherwise) for the double occupancy $\langle n_{i\uparrow} n_{i\downarrow} \rangle$. This is equivalent to the potential or Hubbard energy if multiplied by U. Also shown is the superconducting order parameter defined as the long-range plateau value of the s-wave pair correlation function, $\chi_{\mathrm{os}}^{\mathrm{plateau}}$. In the inset to Fig. 2 we show for comparison the temperature dependence of the order parameter described with the BCS formalism for this parameter regime. Both sets of QMC data, double occupancy *and* superconducting order parameter, show clear transition features exactly in the temperature range where the spin susceptibility goes to zero. In this regime the order parameter increases from zero, and the double occupancy d goes up again (compare inset to Fig. 10, double occupancy in BCS), therefore deviating from the free-system behavior and accounting for an increasing number of double-occupied sites, i.e., pairs. This accounts only for a $\langle \Delta^2 \rangle / U^2$ contribution to the normal-state background, with Δ being the usual superconducting order parameter as for example in BCS theory (see inset of Fig. 2). The three features in the susceptibility, the order parameter and the double occupancy take place exactly at the same temperature, which we would like to define as the critical or superconducting transition temperature T_c, with the same transition region. Therefore we come to the following conclusion: Pair ''formation'' and ''condensation'' take place more or less at the same temperature, $T_p \approx T_c$; the formation of pairs (signaled by d and χ_s) is intimately connected with the transition of the system into a macroscopic coherent quantum state. The deviation of χ_s from the free-system and RPA behavior above T_c results in this (weak) coupling regime from superconducting fluctuations in a critical region around T_c, and is probably not yet connected to a pronounced independent formation of bound pairs above T_c. The mean-field critical temperature resulting from the simple BCS ansatz is $T_c^{\mathrm{BCS}}/t = 0.36$ (see Fig. 2, inset). This is much higher than the QMC estimate, and in this regime one would probably assign the region roughly between the mean-field T_c and the exact T_c to superconducting fluctuations. Treatment within the moment approach using a two-pole ansatz above T_c and four poles in the superconducting region yields comparable results, as shown in Figs. 3 and 4, where we provide again data for the double occupancy and additionally for the chemical potential, which is needed to guar-

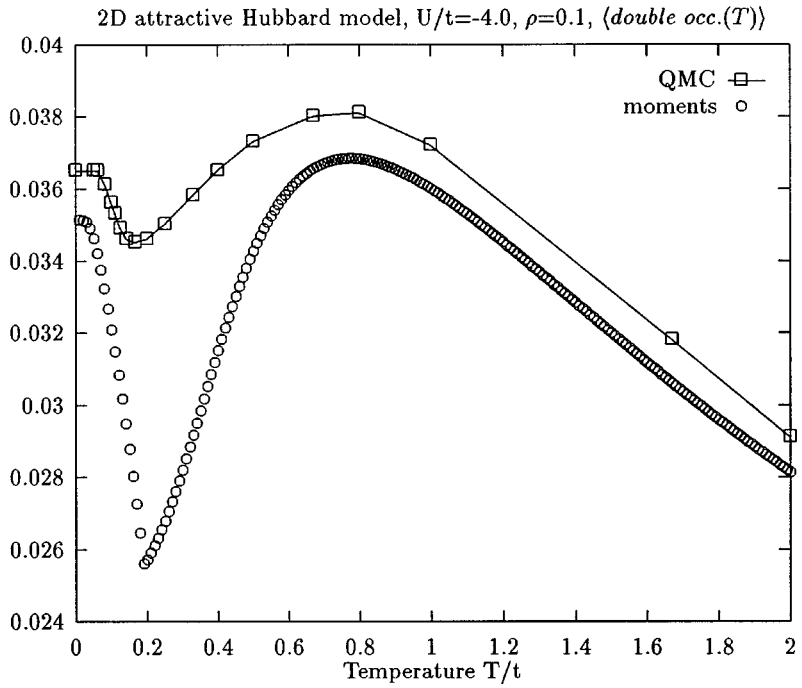

FIG. 3. Temperature dependence of the double occupancy within a QMC simulation (squares) and in the moment approach (circles) with a two-δ-peak ansatz above the transition temperature and a four-peak ansatz in the superconducting regime. System parameters: $U/t=-4.0$, $\rho=0.1$, cluster size in the QMC simulation: 12×12.

antee a fixed density $\rho=0.1$. QMC as well as the moments and also the T matrix[33] reproduce consistently a maximum around $T=0.7t$, which we interpret as a feature of the interacting electron system in the normal state, not related to the appearance of superconductivity. Reference 33 shows that this feature can be explained in terms of a two-excitation-branch ansatz, and provides results for the contributions of the two branches to the double occupancy as a function of temperature. For comparison the double occupancy of the noninteracting one-band system in the normal state can be seen in Fig. 10. This ansatz affords us an excellent understanding of the qualitative behavior of our QMC results because it clearly resembles the most prominent feature in d, which is the increase of the pair number at T_c (again compare with the BCS data in Fig. 10).

The moment approach as well as the even simpler BCS ansatz treat the superconducting phase with a gap separately from the normal, gapless phase. Therefore in these approaches there is no transitional region of superconducting fluctuations, giving rise to a quite sharp feature at T_c, which is smeared out in the QMC data. Otherwise we regard the agreement between the simple δ-peak ansatz of the moment approach and the QMC treatment in this regime to be astonishingly good. It is now important to compare the behavior of μ with the double-occupancy curve. The kink in the moment curve for d also produces a kink in the corresponding

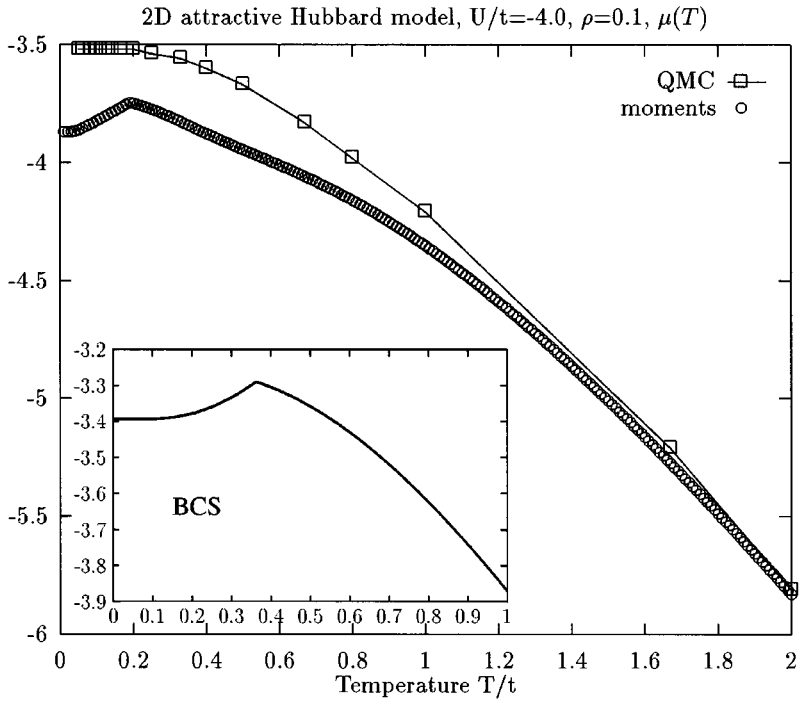

FIG. 4. Temperature dependence of the chemical potential $\mu(T)$, which is necessary to guarantee a constant filling $\rho=0.1$. Coupling strength $U/t=-4.0$. Shown are QMC data (squares, 12×12 lattice), moment data (circles, two-pole ansatz above, four-pole ansatz below the transition) and BCS values in the inset.

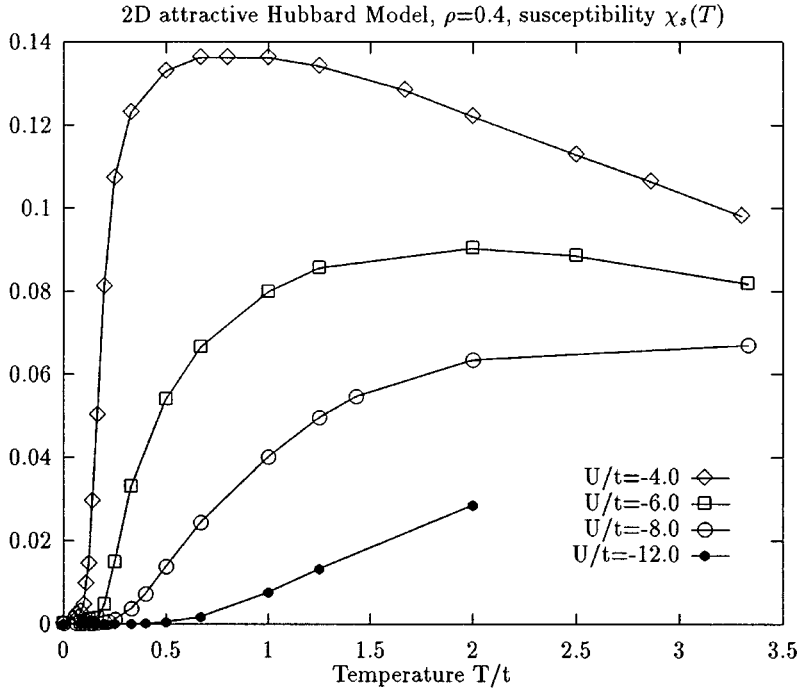

FIG. 5. Uniform magnetic susceptibility χ_s as a function of temperature, $\rho=0.4$ (i.e., 20% doping away from half-filling) for a range of coupling strengths, $U/t=-4.0$ (half of bandwidth $W=8t$) $\rightarrow$ $U/t=-12.0$ ($1.5W$). QMC data, system size 12×12 (144 sites).

μ data because the presence of pairs results in a drop of μ. In the small U moment ansatz the behavior of the chemical potential (i.e., the kink at T_c) agrees with recent findings of van der Marel and Rietveld;[37] we are not able to extract this tiny feature, which we also find within the BCS treatment, from our finite cluster QMC calculation. This might be due to several reasons, one being the smearing out of this detail due to thermal fluctuation region, the other being finite-size effects, the latter being more probable.

So far we have attempted to classify our QMC data in the context of other methods; we shall henceforth switch to the regime close to half-filling, $\rho=0.4$ corresponding to a doping of $\delta=20\%$ away from half-filling, and describe the crossover from weak to strong coupling. This regime is no longer realistically accessible by the other approaches.

B. Crossover

We will first present a number of results, describe them and draw pertinent conclusions in Sec. VI.

1. Magnetic susceptibility

Again starting with the simple uniform static magnetic susceptibility χ_s, Fig. 5, we find for $U/t=-4$ a slightly

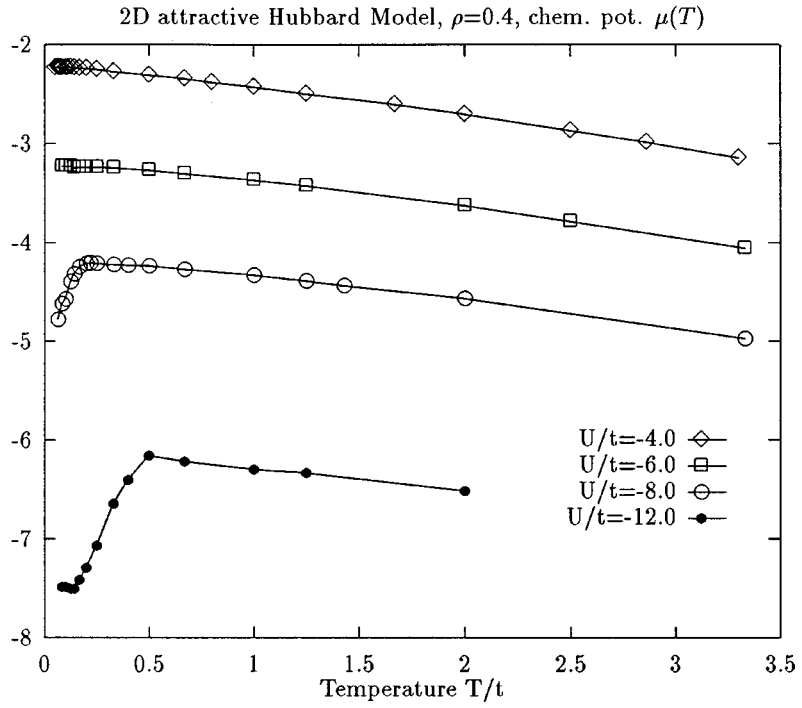

FIG. 6. Temperature dependence of the chemical potential $\mu(T)$, $\rho=0.4$, $U/t=-4.0$, -6.0, -8.0, -12.0, QMC data, system size 12×12.

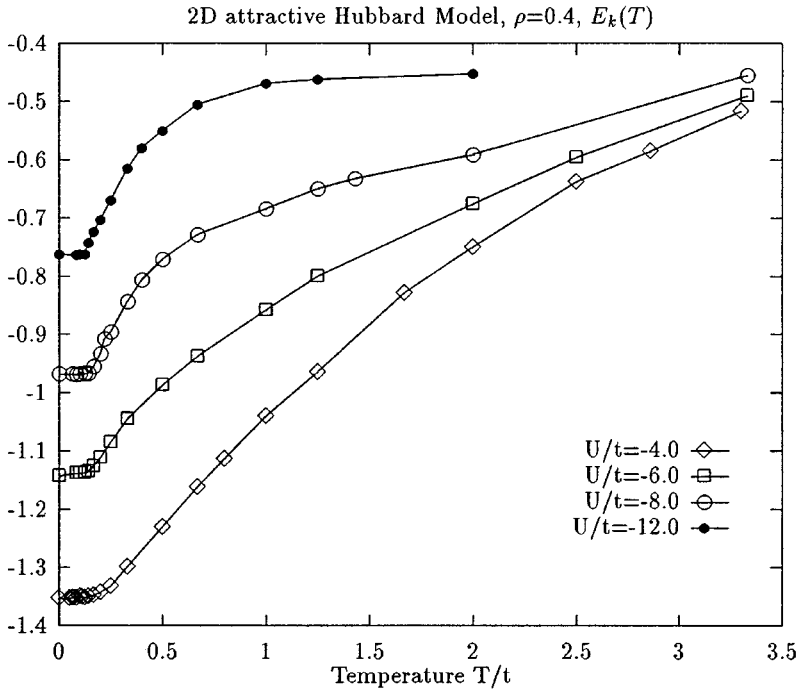

FIG. 7. Kinetic energy $E_k(T)$ as a function of temperature; QMC data, system parameters as in Fig. 6.

enhanced but still similar behavior compared to that in Fig. 1. The situation changes dramatically if one considers higher coupling strengths: The decrease of χ_s starts at very high temperatures and for $U/t \geq 8$, χ_s is an increasing function of T in the temperature regime investigated. Spin excitations are suppressed with decreasing temperature, and we obtain tightly bound pairs which contribute only when they are ionized (''pair breaking''). Obviously we also obtain a new high-temperature scale of coupled spins, i.e., pairs. These results are in very good agreement with Randeria's recent publication (e.g., Ref. 8) for the quarter-filled system, $\rho = 0.25$ (see inset of Fig. 14).

2. Chemical potential

Figure 6 shows the temperature dependence of the chemical potential $\mu(T)$, which is necessary to obtain a certain constant filling, in our case $\rho = 0.4$, for the same set of U values as before. All data shown include for convenience the usual shift $-U/2$, which is not written in the formulation of the initial Hamiltonian in Sec. II; the inclusion of this shift should help the reader compare our data to other, previously published sources, although from a technical point of view the simulation uses the formulation described in Sec. II.

The $(U/t = -4)$ curve shows the usual monotonic behavior. However for large $|U/t| \geq 8$, being comparable to or

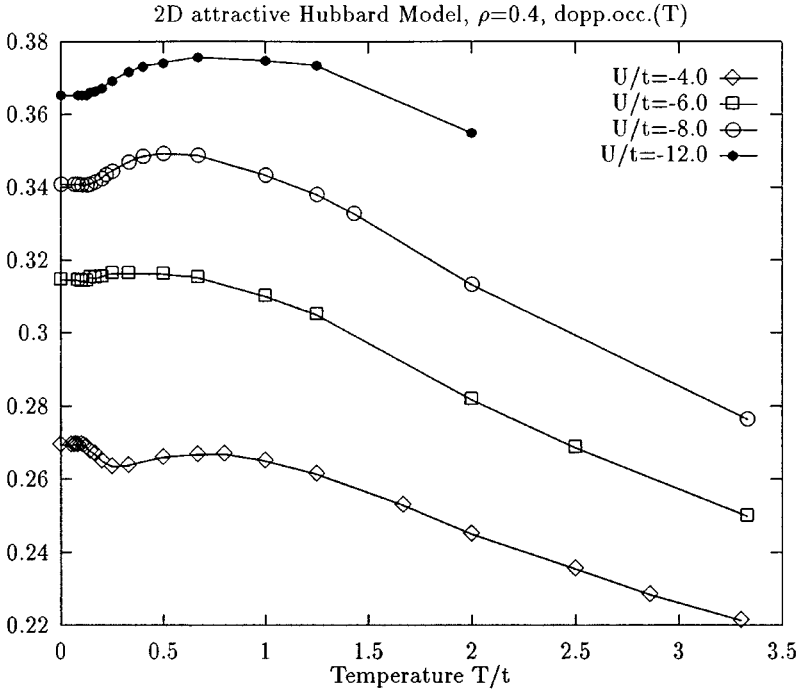

FIG. 8. Double occupancy (potential energy contribution divided by the interaction) as a function of temperature; QMC data, system parameters as in Fig. 6.

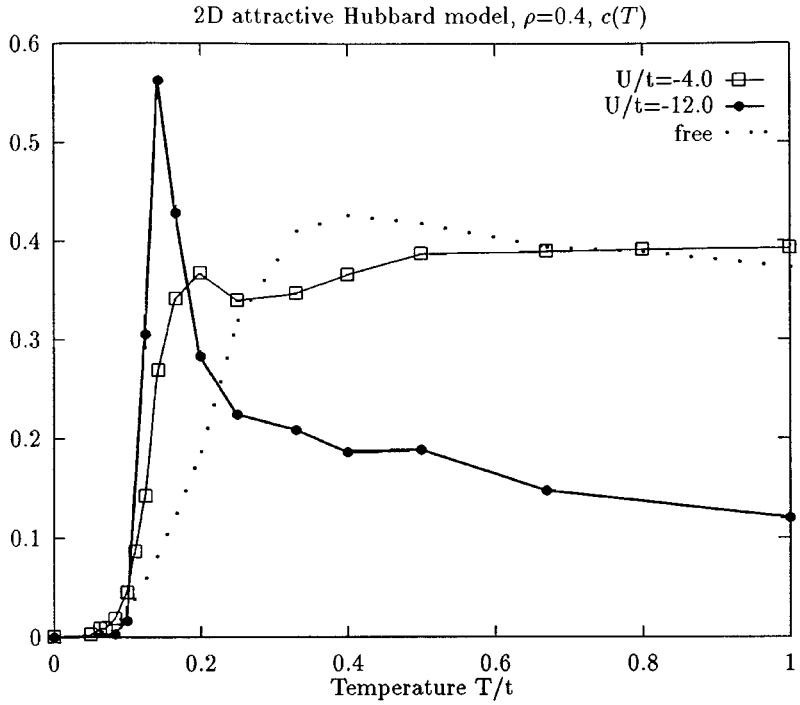

FIG. 9. Temperature dependence of the specific heat $c(T)$, $\rho=0.4$, for the two opposite coupling regimes, weak coupling $U/t=-4.0$ (open squares) and strong coupling $U/t=-12.0$ (filled circles). The dotted line includes, for comparison, the data for the free system, $U/t=0$. QMC data, system size 12×12.

larger than the bandwidth $W/t=8$ of the system, an entirely new and different effect can be seen; $\mu(T)$ decreases with decreasing temperature, whereas in the high-temperature regime a behavior similar to the weak-coupling case is found. Looking at the bending temperature in the $(U/t=-12)$ case, this takes place at an enormously high temperature of $T/t\approx0.5$ and is definitely not related to the transition to the superconducting state.

At this point it is appropriate to comment on the paper of Randeria *et al.*[8] They do not find this feature, and we believe we can explain why not. First, they give a ground-state point at every curve, but it results only from a mean-field approach and is not necessarily an appropriate continuation of QMC data. Second, in the $(U/t=-8)$ case, their QMC data stop at a temperature above the one at which we find the bending of our curve; nevertheless, a continuation of their high-temperature curve into the mean-field ground-state point shows a slight deviation of their low-temperature QMC data, which is in agreement with our results. Third, for $U/t=-12$, in contrast to their other results, they provide data for only an extremely small 4×4 system. We can reproduce their results for $\rho=0.25$ as well as in the $(\rho=0.4)$ case shown by taking the same small 4×4 cluster, but we obtain the bending behavior for larger lattice sizes. It starts to stabilize above a linear dimension of at least 8. We believe that our QMC algorithm is still numerically very stable at this

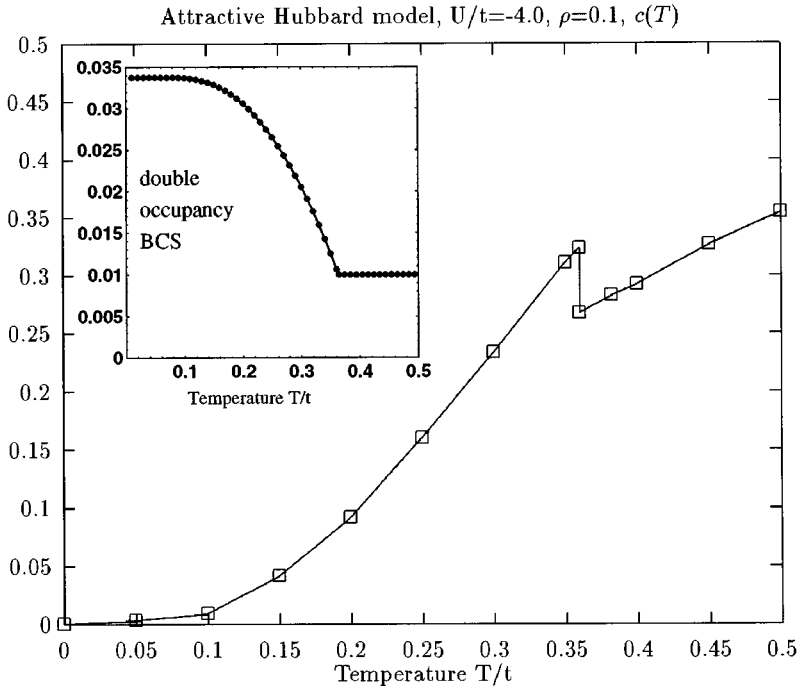

FIG. 10. Temperature dependence of the specific heat $c(T)$ within a BCS ansatz, for a coupling strength of $U/t=-4.0$ and $\rho=0.1$. There is a clear ''mean-field''-like jump at the transition. The inset shows BCS data for the double occupancy; the uprising detail (''finger'') below the transition (pairing instability signal) is responsible for the specific-heat jump.

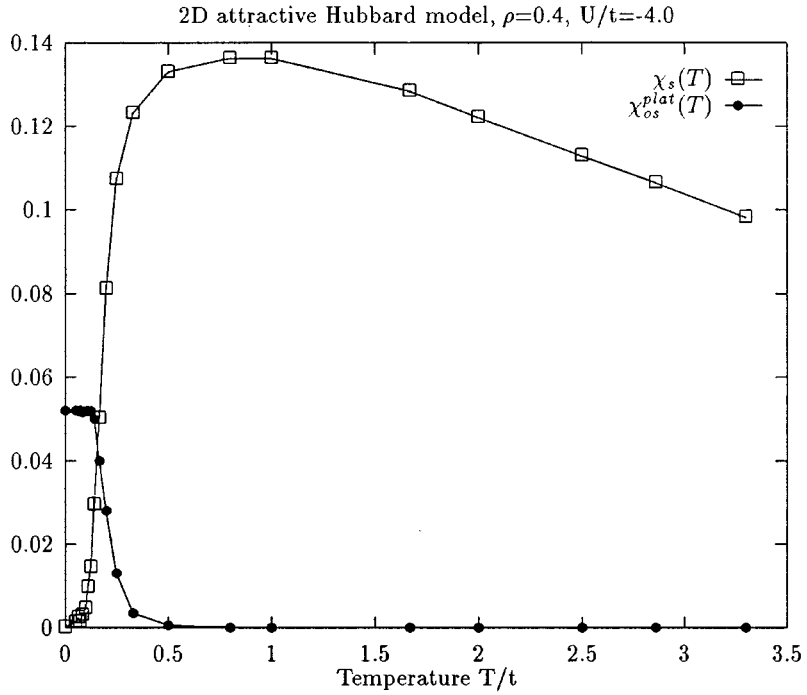

FIG. 11. Temperature dependence of the magnetic susceptibility χ_s (open squares) and the superconducting order parameter χ_{os}^{plat} (filled circles) in the weak-coupling regime $U/t=-4.0$, $\rho=0.4$. QMC data, system size 12×12. Note the coincidence of pairing and condensation temperatures.

strong-coupling strength and low temperatures, which we attempted to monitor with a number of technical indicators and to verify by a comparison of several observables to results from other (e.g., exact diagonalization) techniques. This bending is also found for the same values of U in the normal-state moment approach, with an uncertainty due to possible numerical artifacts in this coupling and temperature regime. In contradiction to the results shown for finite dimensions, a simulation of an infinite-dimensional system after Hirsch and Fye[38] and Georges and Krauth,[39] where a mean-field-like treatment becomes exact, does not reveal this bending and yields a monotonic behavior. Therefore, we cannot definitely clarify whether the QMC results simply reproduce an artifact of the method, or whether the shown properties are a true feature of a finite-dimensional system; a more detailed discussion of this subject will be presented in a future publication.[40]

Our interpretation of this phenomenon is that the formation of tightly bound pairs above the condensation temperature, as already indicated by the spin susceptibility, leads to this reduction. In a simple intuitive description this pair formation obviously has a certain influence on the chemical potential of the *electrons* because a fraction of the fermions is tightly coupled into local composite bosons. Therefore the effective filling of the remaining fermionic system decreases, which involves a decrease of the chemical potential. The S

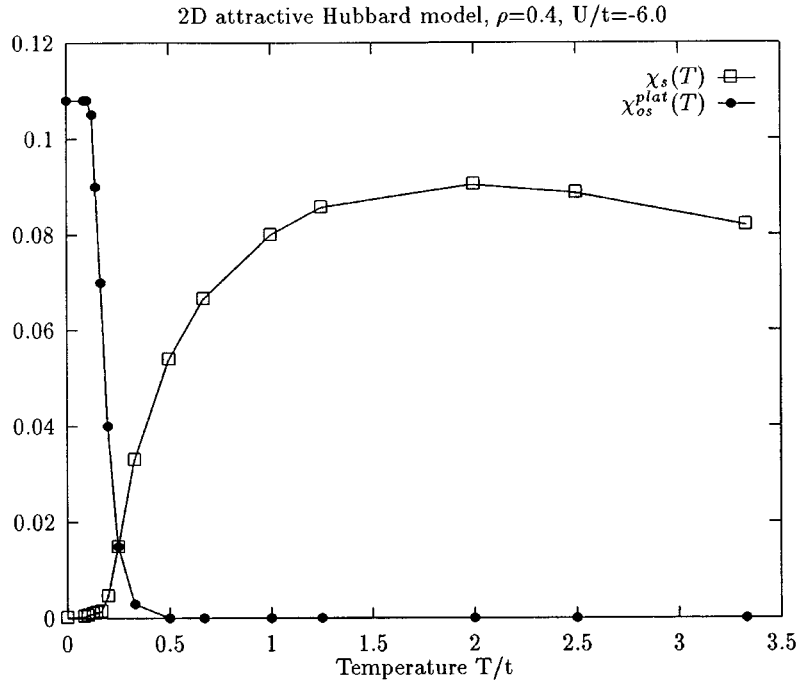

FIG. 12. Temperature dependence of the magnetic susceptibility χ_s (open squares) and the superconducting order parameter χ_{os}^{plat} (filled circles) for an intermediate-coupling strength $U/t=-6.0$, $\rho=0.4$. QMC data, system size 12×12.

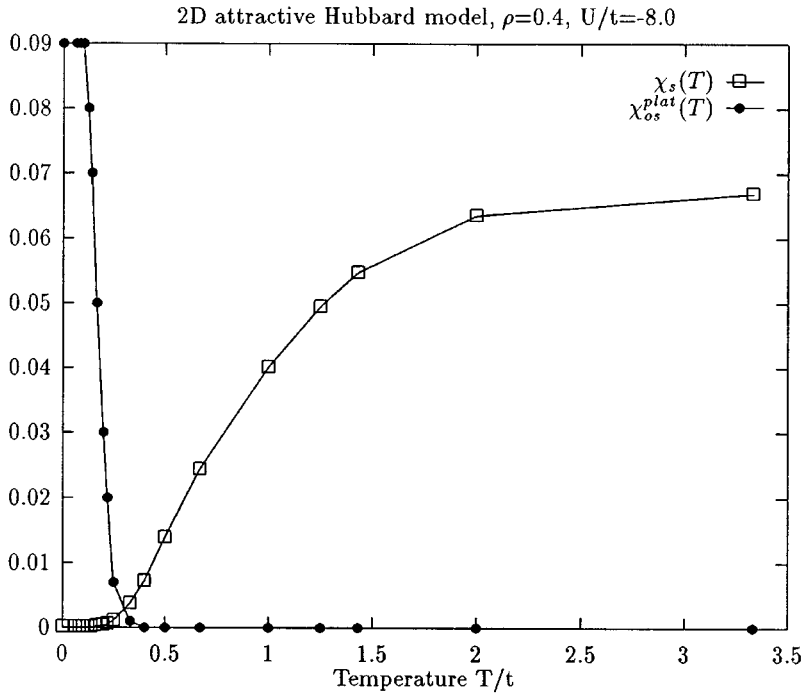

FIG. 13. Temperature dependence of the magnetic susceptibility χ_s (open squares) and the superconducting order parameter $\chi_{\mathrm{os}}^{\mathrm{plat}}$ (filled circles) in the strong-coupling regime $U/t=-8.0$ (bandwidth $W=8t$). The temperatures for pair formation (indicated by the decrease of the susceptibility down to zero) and condensation (indicated by the order parameter) are clearly separated, in contrast to Fig. 11, $U/t=-4.0$. QMC data, system size 12×12.

shape of the curve, i.e., the back bending at very low temperatures, merely reflects that only a certain portion of the electrons are constituents of the bosonic pairs, whereas the remaining electrons contribute to the fermionic system, and the chemical potential of the fermions remains finite. This is an indication that we are somehow still in an intermediate regime, where only a part of the fermionic system is tightly paired. We expect this portion to increase with increasing attractive coupling. The effect described fits, in our opinion, very well into the picture of a formation of composite bosons far above a superconducting transition.

3. Energies

We now turn to the temperature dependence of the two constituents of the total energy, the kinetic energy and the potential contribution, or rather its descendant, the double occupancy. Looking at Figs. 7 and 8, which show these dependences for the same U values as in the case of the susceptibility and the chemical potential, one can immediately see the qualitative crossover between weak- and strong-coupling data. We first discuss the double occupancy, Fig. 8: Whereas in the case of $U/t=-4.0$ we find the already discussed increase at T_c, there is now a change in the low-temperature behavior of d for $U/t=-12.0$, d simply approaches a constant value. This is the important difference. The fact, that we still find a maximum of d at high temperatures reproduces a relic of the free system because at these temperatures we have a dynamic double occupation, an effect we would also see in a nonsuperconducting system. This detail should disappear for a higher coupling strength because for infinitely strong coupling we would get $d=\rho$.

In the potential energy part the characteristic feature disappears, and in the kinetic term a new one arises when we move through the crossover regime towards large U. We can extract this from the data in Figs. 7 and 8. Starting again from small U the kinetic energy merely behaves like in the free system; in contrast, the large-U data are qualitatively different, because the kinetic energy becomes more or less constant over a large temperature range, and it gets closer and closer to zero. We interpret this as a vanishing of the kinetic energy of the fermions due to a strong pair coupling. When the composite bosonic pairs undergo a phase transition into a condensed phase-coherent state, the fermions as their constituents regain kinetic energy. Such behavior is reminiscent of the behavior of preformed pairs; at T_c the specific heat has a peak. The transition occurs over quite a large range due to a large fluctuation region; we will comment on this later.

4. Specific heat

The aforementioned behavior of the kinetic and potential energies will also be reflected in the specific heat, shown in Fig. 9 for $U/t=-4$ and $U/t=-12$. For weak and intermediate coupling ($U/t=-4$) we observe qualitative agreement with a BCS jump, illustrated in Fig. 10. In the QMC data the jump is smeared out by finite-size effects in our still very small system. This is well documented also in classical and quantum spin systems, where a ''real'' discontinuous jump could be only expected in the case of an infinite system, so a size scaling would be necessary for an appropriate treatment and will be done in the near future.

In contrast the large-U case shows a totally different curve, and reflects much better the predicted specific-heat behavior of a local pair system in $D=3$, which will exhibit a logarithmic anomaly at the condensation temperature.[4] The specific heat of such a system is proportional to T^3 below the λ singularity for $T\rightarrow0$ as well as to a behavior $\propto1/T^2$ above the singularity in the normal state $T\rightarrow\infty$.

One strong advantage of our numerical access to this intricate problem of describing a crossover phenomenon becomes obvious: We are not only able to provide results for the specific heat in the two limiting cases, we can also assign this qualitative change to specific effects in the underlying constituents of the energy, i.e., the increase of pairs at T_c in

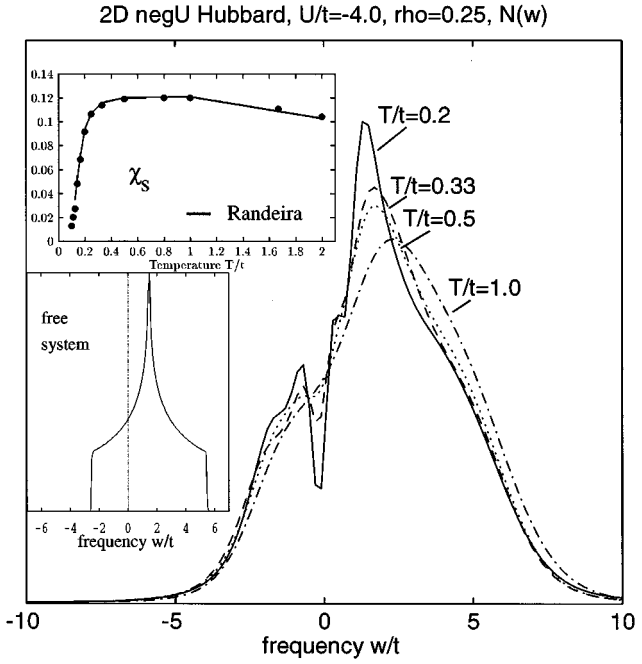

FIG. 14. Single-particle density of states $N(\omega)$ above the superconducting transition, weak coupling $U/t=-4.0$, quarter filling $\rho=0.25$, for a number of temperatures far above the transition in the normal state, $T/t=0.2$ (solid line), $T/t=0.33$ (dashed line), $T/t=0.5$ (dotted line) and $T/t=1.0$ (dash-dotted line). QMC data, system size 10×10, analytic continuation via MaxEnt. The frequencies, measured in units of t, are counted so that the chemical potential corresponds to $\omega/t=0$. The upper inset shows the temperature dependence of the uniform magnetic susceptibility $\chi_s(T)$ (filled circles) from our simulations; for comparison, data from Randeria *et al.* (Ref. 8) is included (solid line). The lower inset figure displays the noninteracting case, $U/t=0$ (''free band''), for the same filling $\rho=0.25$.

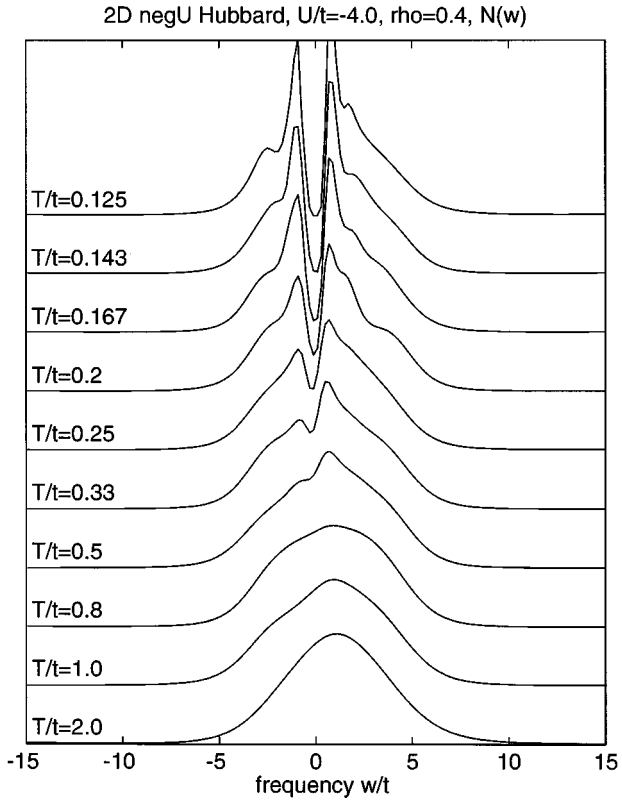

FIG. 15. Single-particle density of states $N(\omega)$, weak coupling $U/t=-4.0$, filling $\rho=0.4$, for a series of temperatures. QMC data, system size 8×8, analytic continuation via MaxEnt.

the BCS case (i.e., the uprising ''finger'' shown in the inset of Fig. 10), and the manifestation of BEC in the kinetic energy in the strong-coupling regime. In contrast to the chemical potential, where we find some principal differences between finite-dimensional QMC simulations and an infinite-dimensional simulation (see above), the discussed qualitative crossover in the specific heat between the weak- and strong-coupling limits is fully supported by recent infinite-dimensional simulations; we again refer to Ref. 40.

Why do we find mean-field-like behavior in the weak-coupling regime that qualitatively and even quantitatively resembles the characteristics of the three-dimensional system? Around the transition temperature T_c we always find a temperature window with superconducting fluctuations. The width of this window strongly increases with increasing coupling strength, and the coherence length and therefore the extension of a singlet pair decreases. In the limit of highly extended pairs a mean-field treatment of the effects becomes increasingly appropriate. This is the reason for the incredible success of the BCS approach in the conventional superconductors with their large coherence lengths and pair extensions. Each pair overlaps with numerous other pairs, and therefore ''lives in the mean field of the others.'' In contrast, short-coherence-length materials with their more or less local pairs obviously show certain differences, which we indeed expect. A system with short coherence length will exhibit a wide critical regime, and its true critical behavior should be observable, whereas in the weak-coupling BCS-like regime the width of the critical regime can be as narrow as 10^{-15} T_c and is usually technically inaccessible.

An elaborate discussion of the differences in critical behavior and the critical exponents can be found in the work of Micnas *et al.*[4] Indeed, one of the remarkable characteristics of the high-T_c materials is their small-coherence-length volume, leading to pronounced thermal fluctuation effects consistent with 3D xy-critical-point behavior.[41]

In addition, the fact that we find the phenomena of the weak-coupling 2D system to be quite similar to the effects expected from a real 3D phase transition supports our argumentation because as long as a mean-field treatment yields the dominant features, the difference between 2D and 3D should play only a minor role, at least concerning the description of certain details. A ''mean field'' should not be able to distinguish dimensionality. We are nevertheless aware of the principle implications of Mermin and Wagner's theorem. With increasing U, features characteristic for a KT-like transition should become more important, and we expect a more pronounced difference between the behavior of the 2D and the 3D system. Up to now, our resolution is too poor to investigate quantitative differences, especially because our systems might be still too small to allow reasonable estimates, for example, of the exact position of the specific-heat peak relative to the transition temperature or of the appropriate critical exponents. To substantiate our argumentation concerning the separation of the two temperature scales for

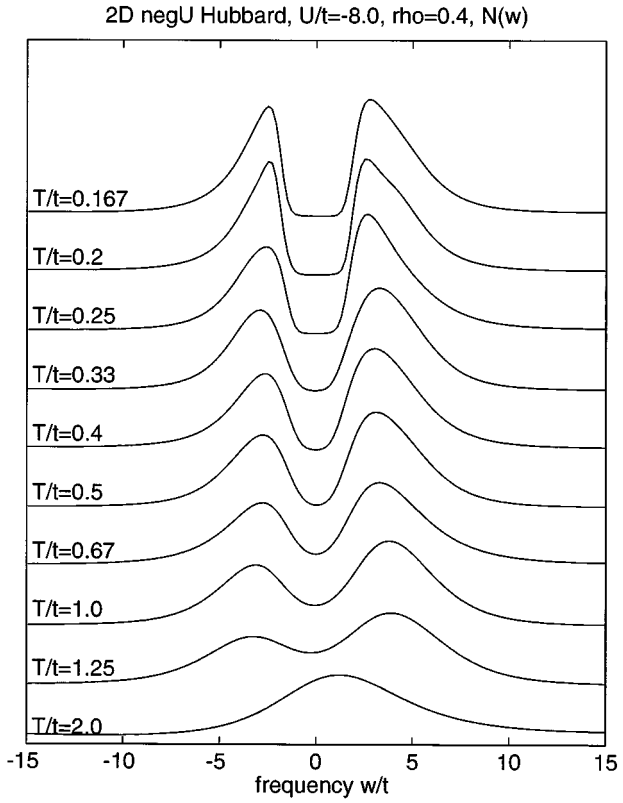

FIG. 16. Single-particle density of states $N(\omega)$, weak coupling $U/t=-8.0$, filling $\rho=0.4$, for a series of temperatures. QMC data, system size 8×8, analytic continuation via MaxEnt.

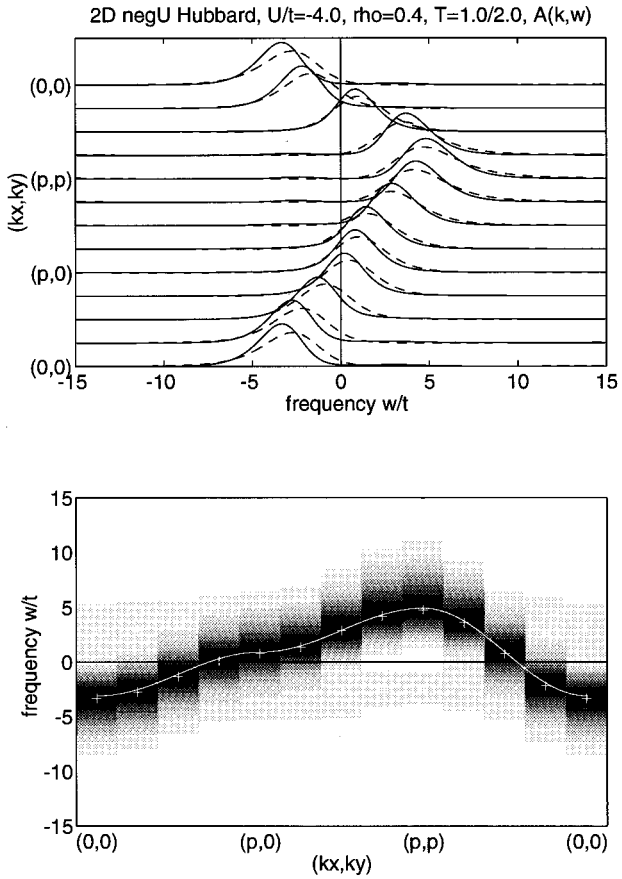

FIG. 17. Momentum-resolved single-particle spectral density $A(\vec{k},\omega)$ versus ω and $\vec{k}=(k_x,k_y)$ along the triangle path (0,0), $(\pi,0)$, (π,π), (0,0) in k space $(\Gamma\rightarrow X\rightarrow M\rightarrow\Gamma)$, weak coupling $U/t=-4.0$, $\rho=0.4$. The upper image contains data for $T/t=2.0$ (dashed lines) and $T/t=1.0$ (solid lines) in the normal state far above T_c. The frequency is measured relative to the chemical potential located at $\omega=0$. Lower image: ''Band-structure'' representation of $A(\vec{k},\omega)$ by gray-scale shading; peak height is coded by dark areas and the peak maximum is marked by a cross. Temperature $T/t=1.0$. For comparison, the cosine dispersion of the free system is included (solid white line).

pair formation and pair condensation in the crossover regime, we again turn away from the energy discussion.

5. Order parameter: pair formation vs condensation

As discussed in the introduction, a common feature of both extremal regimes, the weak-coupling BCS and the strong-coupling BEC description, is the fact that in both cases we can apply Yang's ODLRO concept[3] in the density matrix, or rather in the pair-correlation function, to identify the appearance of a macroscopic quantum state (superfluidity or superconductivity). Therefore we take this indicator to investigate the superconducting transition–condensation temperature T_c (or T_{KT}).

On the other hand, a good indicator of pair formation are the simple uniform magnetic susceptibility χ_s, as discussed above, and the single-particle momentum-resolved spectral densities and single-particle densities of states. First we concentrate on χ_s. Figures 11–13 show for $U/t=-4$, -6, -8 the behavior of the plateau value of the s-wave singlet pair correlation function $\chi_{\mathrm{os}}^{\mathrm{plat}}$ as an ODLRO indicator and therefore as the order parameter for the condensation transition as a function of temperature. All three curves include additionally the corresponding spin-susceptibility data.

The results are quite obvious: Whereas in the $(U/t=-4.0)$ case (Fig. 11) the formation of pairs, indicated by the bending down of χ_s, and the transition into the macroscopic quantum state, signaled by the increase of $\chi_{\mathrm{os}}^{\mathrm{plat}}$, appear to take place at more or less the same temperature, both effects seem to separate into two distinct effects at different temperatures when we go via $U/t=-6$ to $U/t=-8$ (Figs. 12 and 13). The latter gives clear evidence of a condensation effect at a temperature far below the one at which the spin excitations are suppressed and bound pairs are formed. Therefore we are able to show not only the strong increase of the pair formation temperature with increasing interaction, but also the separation of the two phenomena, namely pair formation and condensation, which are no longer intimately connected in the strong-coupling regime.

6. Spectral properties

The pair formation described should also be observable in the single-particle fermionic density of states because the formation of coupled pairs due to an interaction U should cause a depletion of certain energetic states and the formation of a gaplike structure. That is indeed what we find; Figs. 14–16 show the densities of states $N(\omega)$ plotted for various different temperatures. The frequencies ω are measured in units of t relative to the chemical potential, which corre-

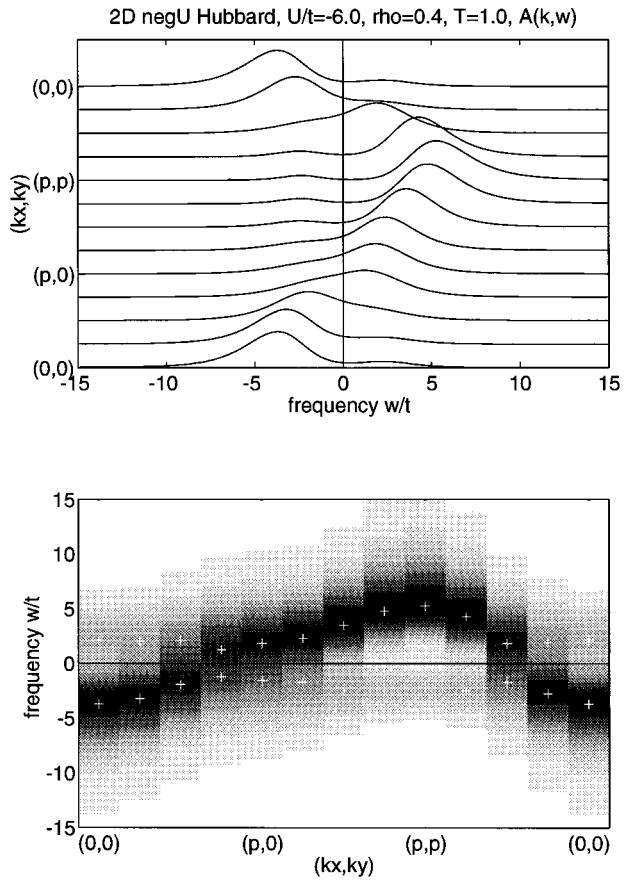

FIG. 18. Momentum-resolved single-particle spectral density $A(\vec{k},\omega)$ versus ω and $\vec{k}=(k_x,k_y)$, similar to Fig. 17, intermediate coupling $U/t=-6.0$, $\rho=0.4$, $T/t=1.0$.

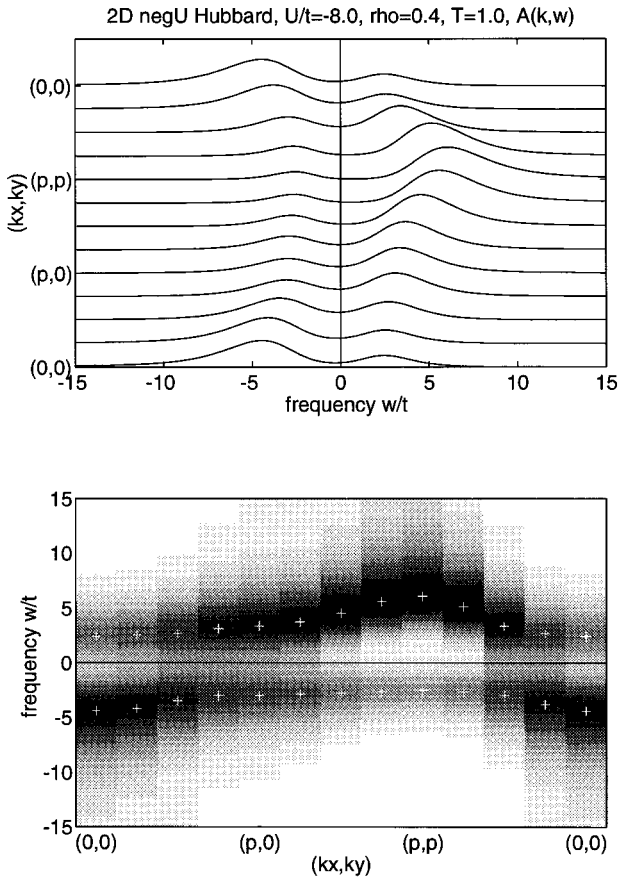

FIG. 19. Momentum-resolved single-particle spectral density $A(\vec{k},\omega)$ versus ω and $\vec{k}=(k_x,k_y)$, similar to Fig. 17, strong coupling $U/t=-8.0$, $\rho=0.4$, $T/t=1.0$.

sponds to $\omega/t=0$. A distinct pseudogap structure appears above T_c in all cases, nicely connected to the corresponding suppression of the magnetic susceptibility, Fig. 14. In Fig. 14 we present data for a quarter-filled system, $\rho=0.25$, to allow the reader to make a direct comparison with data in other recent publications, e.g., Ref. 8. This ''normal-state gap'' structure is extremely pronounced in the case of strong coupling, even for high temperatures above $T/t=1.0$, whereas the condensation temperature would be in the regime around $T/t=0.1$ or even below, lower by roughly a factor equal to or larger than 10. In the case of $U/t=-8$ (Fig. 16) a clear gap in the single-particle electronic density of states with a flat bottom around frequency $\omega=0$ is found for temperatures $T/t\approx 0.25$, still much higher than the condensation temperature, giving rise to the assumption that we are left with very tightly bound pair states.

For a last but very essential property, we present results for the single-particle momentum-resolved spectral densities $A(k,\omega)$ and the associated peak position and amplitude dispersions in momentum space above the condensation temperature, $-4\geqslant U/t\geqslant -12$, and attempt to explain them in terms of pair formation using information known from the simple moment approach[33,34] (Figs. 17–20). The figures provide information for $A(k,\omega)$ along the usual triangle in k space, i.e., $(0,0)\rightarrow(\pi,0)\rightarrow(\pi,\pi)\rightarrow(0,0)$. Figure 17 shows data for the low coupling parameter set $U/t=-4.0, T/t=2.0$, i.e., a very high temperature. We find more or less the total spectral weight concentrated in a free-system-like one-band structure, which fits ideally the usual cosine band of free fermions on a 2D lattice if we take the dispersion of the peak positions from the QMC spectral densities (see lower part of Fig. 17). This does not change remarkably when we go to a higher coupling strength, at least in the investigated regime up to $U/t=-12$, which leads us to the conclusion that at this high temperature the system follows a band of merely unpaired, free-system-like fermions. The situation changes when we go to lower temperatures, $T/t=1.0$. In the $(U/t=-4.0)$ case this change is not dramatic because only a small secondary peak structure with nearly vanishing weight arises in the region around momentum (0,0) and (π,π). This small weight transfer signals a small occupation of that band far above T_c, which we associate with pair excitations, and probably outside the temperature window of mere critical fluctuations. Therefore we find ourselves already in the onset regime of pair formation and thus at the beginning of the crossover from BCS superconductivity to BEC because we find a coexistence of still dominating BCS-like features and effects resulting from the appearance of firmly coupled pairs above T_c. Increasing coupling strength causes an increased population of the second excitation branch, resulting in a band having pair characteristic with nonvanishing spectral weight in the normal state at increasing temperature, accompanied by an increasing separation of both bands leading to the final appearance

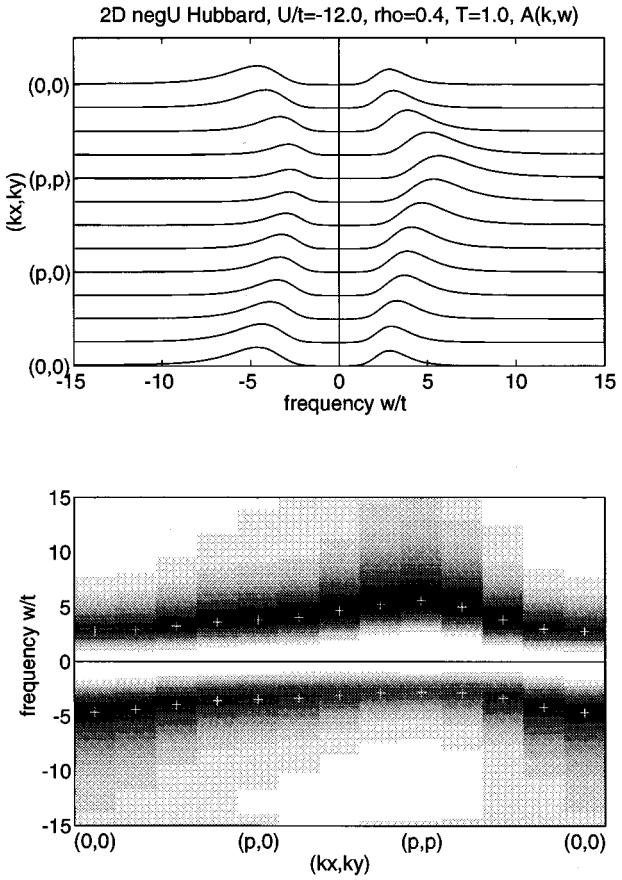

FIG. 20. Momentum-resolved single-particle spectral density $A(\vec{k},\omega)$ versus ω and $\vec{k}=(k_x,k_y)$, similar to Fig. 17, strong coupling $U/t=-12.0$, $\rho=0.4$, $T/t=1.0$.

of a gap around $\omega=0$, which is first indicated in the case of $U/t=-6.0$ by the precursor-like splitting of the peaks around $(\pi,0)$ and $(\pi/2,\pi/2)$. We wish to mention the important result that this gap is not due to superconductivity or condensation effects because we are still dealing with the regime at least one order of magnitude above the condensation temperature. Rather, this gap is a pure correlation effect caused by the attractive interaction U, which leads to the splitting of the band system. We would like to connect these two bands with a single-particle band and a pair band, which become increasingly separated with increasing U, and which are additionally subjected to a growing weight transfer from the single-particle to the pair band, i.e., the appearance of a growing proportion of tightly bound composite pairs. Recall that this effect is accompanied by a strong suppression of the magnetic response (Fig. 5). To clarify the effects discussed above, we include the band structures for $T/t=2.0$ and $T/t=1.0$ and coupling strengths $U/t=-4.0$, -6.0, -8.0, -12.0 in the lower parts of Figs. 17–20, respectively, which we obtain if we use a gray-scale type of coding for $A(k,\omega)$ and mark the k dispersion of the peaks of the reconstructed QMC spectral densities. The dispersion of the spectral peak amplitudes $\alpha_i(k)$ can also be seen in these gray-coded pictures, where the white parts correspond to zero and an increasing gray level to increasing amplitude. The crossover effect can be nicely seen in Fig. 18. This interpretation seems to be in agreement with the moment and T-matrix calculations[33] above the condensation temperature, and the appearance of two excitation branches is remarkably consistent with results from the other methods, namely the T-matrix approach. Nevertheless we would like to state that there are some qualitative differences in the shape of the dispersion resulting from QMC simulations and the bands obtained by the simple δ-peak ansatz.

VI. SUMMARY

We presented extended quantum Monte Carlo data for various static and dynamic properties of the attractive Hubbard model. Particular emphasis was placed on the crossover from BCS-like superconductivity to the Bose-Einstein condensation of local pairs. The observables investigated include magnetic susceptibilities, energies, specific heat, order parameters, and spectral properties. First, the dominant effect in the crossover region is the appearance of more or less tightly bound pairs (far) above the superconducting transition, for which we found a number of manifestations in several of the quantities described. We have been able to observe and quantify the separation of the formation of pairs and the condensation of the pairs into a coherent state with increasing coupling strength. In the weak-coupling limit, the scenario is intimately connected to the Fermi surface instability hypothesis of the BCS theory, whereas in the strong-coupling regime the two effects, pair formation and pair condensation, are no longer connected at all and can take place at different temperatures. Correlated to the formation of pairs in the normal state above T_c is the downward bending of the static spin susceptibility and the appearance of a pseudogap structure in the single-particle electronic density of states. Moreover the attractive interaction gives rise to a pair formation in the normal, nonsuperconducting state, leading to an energy band of paired electrons. For weak and intermediate interactions this band overlaps and hybridizes with the free quasiparticle band, whereas in the case of strong coupling we find two distinct and separate bands. The crossover takes place in the coupling range between $W/2$ and W, where W is the bandwidth of the system. Both effects, the spin-gap and the pseudogap in the density of states, are documented in our data. Where applicable, the comparison between the presented QMC data and the results of other methods is surprisingly good, which justifies the interpretation of the QMC data in terms of knowledge resulting, for example, from the quite simple δ-peak ansatz of the moment method.

ACKNOWLEDGMENTS

We thank Ch. Baur, W. Fettes, T. Hußslein, P. F. Meier, R. Micnas, I. Morgenstern, J. J. Rodríguez-Núñez, and S. Schafroth for useful discussions, as well as W. von der Linden for helpful support with the maximum entropy technique. This work was funded by the Swiss National Fund, and the simulations have been performed on the IBM SP-2 Power Parallel System at the Computing Center of the University of Zürich (RZU); the generous funding and the CPU grant are gratefully acknowledged. We thank IBM Research for help and hospitality.

[1] See, e.g., D. R. Tilley and J. Tilley, *Superfluidity and Superconductivity* (IOP, London, 1994).
[2] See, e.g., J. Blatt, *Theory of Superconductivity* (Academic, New York, 1964); M. R. Schafroth, Phys. Rev. **100**, 463 (1955).
[3] C. N. Yang, Rev. Mod. Phys. **34**, 694 (1962).
[4] R. Micnas, J. Ranninger, and S. Robaszkiewicz, Rev. Mod. Phys. **62**, 113 (1990).
[5] A. J. Leggett, J. Phys. (Paris) Colloq. **41**, C7-19 (1980); in *Modern Trends in the Theory of Condensed Matter* (Springer, Heidelberg, 1980).
[6] P. Noziers and S. Schmitt-Rink, J. Low Temp. Phys. **59**, 95 (1985).
[7] R. Hausmann, Z. Phys. B **91**, 291 (1993).
[8] M. Randeria, N. Trivedi, A. Moreo, and R. T. Scalettar, Phys. Rev. Lett. **69**, 2001 (1992).
[9] M. Randeria, in *Bose-Einstein Condensation*, edited by A. Griffin *et al.* (Cambridge University Press, Cambridge, England, 1994).
[10] R. dos Santos, Phys. Rev. B **50**, 635 (1994).
[11] J. E. Hirsch, Phys. Rev. B **31**, 4403 (1985).
[12] H.-G. Matuttis, Ph.D. thesis, University of Regensburg, 1995.
[13] A. Moreo and D. J. Scalapino, Phys. Rev. Lett. **66**, 946 (1991).
[14] T. Schneider, H. Beck, D. Bormann, T. Meintrup, S. Schafroth, and A. Schmidt, Physica C **216**, 432 (1993).
[15] G. Sugiyama and S. E. Koonin, Ann. Phys. **168**, 1 (1986).
[16] S. Sorella, S. Baroni, R. Car, and M. Parinello, Europhys. Lett. **8**, 663 (1989).
[17] H. deRaedt, Comput. Phys. Rep. **7**, 1 (1987).
[18] J. E. Hirsch, Phys. Rev. B **38**, 12 023 (1988).
[19] E. Y. Loh Jr., J. E. Gubernatis, R. T. Scalettar, R. L. Sugar, and S. R. White, in *Workshop on Interacting Electrons in Reduced Dimensions*, edited by D. Baeriswyl and D. K. Campbell (Plenum, New York, 1989).
[20] M. Ulmke and H. Müller-Krumbhaar, Z. Phys. B **86**, 383 (1992).
[21] R. Blankenbecler and R. L. Sugar, Phys. Rev. D **27**, 1304 (1983).
[22] M. Imada, J. Phys. Soc. Jpn. **57**, 2689 (1988); **58** 3752 (1989).
[23] W. Kohn and D. Sherrington, Rev. Mod. Phys. **42**, 1 (1970).
[24] G. L. Sewell, J. Stat. Phys. **61**, 415 (1990).
[25] H. T. Nieh, G. Su, and B.-H. Zhao (unpublished).
[26] W. von der Linden, Phys. Rep. **220**, 53 (1992).
[27] Ch. Baur, Diploma thesis, University of Regensburg, 1994.
[28] J. Gubernatis, M. Jarrell, R. N. Silver, and D. S. Sivia, Phys. Rev. B **44**, 6011 (1991).
[29] M. Jarrell (unpublished); M. Jarrell and J. Gubernatis, Phys. Rep. **269**, 133 (1996).
[30] B. Buck and V. A. Macaulay, in *Maximum Entropy in Action* (Oxford University Press, Oxford, 1990).
[31] W. von der Linden (unpublished).
[32] W. Nolting, *Vielteilchentheorie* (Verlag Zimmermann-Neufang, Ulmen, 1991).
[33] T. Schneider, M. H. Pedersen, and J. J. Rodríguez-Núñez, Z. Phys. B (to be published).
[34] M. Pedersen, T. Schneider, J.J. Rodríguez-Núñez, and H. Beck (unpublished).
[35] R. Micnas, M. H. Pedersen, S. Schafroth, T. Schneider, J. J. Rodríguez-Núñez, and H. Beck, Phys. Rev. B **52**, 16 223 (1996).
[36] A. Moreo, D. J. Scalapino, and S. R. White (unpublished); Phys. Rev. B **45**, 7544 (1992).
[37] D. van der Marel and G. Rietvield, Phys. Rev. Lett. **69**, 2575 (1992).
[38] J. E. Hirsch and R. M. Fye, Phys. Rev. Lett. **56**, 2521 (1986).
[39] A. Georges and W. Krauth, Phys. Rev. Lett. **69**, 1240 (1992).
[40] M. H. Pedersen *et al.* (unpublished).
[41] T. Schneider and H. Keller, Int. J. Mod. Phys. B **5**, 487 (1993).